









Virtual Outcrops Building in Extreme Logistic Conditions for Data Collection, Geological Mapping, and Teaching: The Santorini's Caldera Case Study, Greece

Fabio Luca Bonali^{1,2}^a, Luca Fallati¹^b, Varvara Antoniou³^c, Kyriaki Drymoni⁴^d,
Federico Pasquaré Mariotto⁵^e, Noemi Corti¹^f, Alessandro Tibaldi^{1,2}^g, Agust Gudmundsson⁴
and Paraskevi Nomikou³^h

¹Department of Earth and Environmental Sciences, University of Milano-Bicocca, Piazza della Scienza 4,
Ed. U04, 20126, Milan, Italy

²CRUST- Interuniversity Center for 3D Seismotectonics with Territorial Applications, Italy

³Department of Geology and Geoenvironment, National and Kapodistrian University of Athens,
Panepistimioupoli Zografou, 15784 Athens, Greece

⁴Department of Earth Sciences, Queen's Building, Royal Holloway University of London, Egham, Surrey TW20 0EX, U.K.

⁵Department of Human and Innovation Sciences, Insubria University, Via S. Abbondio 12, 22100 Como, Italy

Keywords: Virtual Outcrops, Photogrammetry, Structure from Motion, Santorini Volcano, Caldera, Dykes.


Abstract: In the present work, we test the application of boat-camera-based photogrammetry as a tool for Virtual Outcrops (VOs) building on geological mapping and data collection. We used a 20 MPX camera run by an operator who collected pictures almost continuously, keeping the camera parallel to the ground and opposite to the target during a boat survey. Our selected target was the northern part of Santorini's caldera wall, a structure of great geological interest. A total of 887 pictures were collected along a 5.5-km-long section along an almost vertical caldera outcrop. The survey was performed at a constant boat speed of about 4 m/s and a coastal approaching range of 35.8 to 296.5m. Using the Structure from Motion technique we: *i*) produced a successful and high-resolution 3D model of the studied area, *ii*) designed high-resolution VOs for two selected caldera sections, *iii*) investigated the regional geology, *iv*) collected qualitative and quantitative structural data along the vertical caldera cliff, and *v*) provided a new VO building approach in extreme logistic conditions.


1 INTRODUCTION


Field studies and data collection are vital components for geological mapping and for understanding the active processes on Earth, with particular regard to shallow magmatic ones (e.g. Tibaldi and Bonali, 2017; Gudmundsson, 2020). Field studies can be


challenging, due to particular field-related conditions, that cause limited outcrop accessibility and result in poor data collection.


Thus, mapping and data collection on Unmanned Aerial Vehicles (UAVs)-based photogrammetry-derived Digital Surface Models (DSMs), Orthomosaics and Virtual Outcrops (VOs), have become standard practice, especially in volcanic areas


^a <https://orcid.org/0000-0003-3256-0793>


^b <https://orcid.org/0000-0002-5816-6316>


^c <https://orcid.org/0000-0002-5099-0351>

^d <https://orcid.org/0000-0001-7262-8719>

^e <https://orcid.org/0000-0003-2157-8760>

^f <https://orcid.org/0000-0002-0798-6429>

^g <https://orcid.org/0000-0003-2871-8009>

^h <https://orcid.org/0000-0001-8842-9730>

(e.g. Bonali et al., 2020; Tibaldi et al., 2020). VOs are also known as digital outcrop models, which are a digital 3D representation of the outcrop surface (e.g Xu et al., 1999). By contrast, static camera-based outcomes are rare and restricted to narrow-sized surveys on small field-scale geological features (e.g. Scott et al., 2020).

In this paper, we test the use of camera-based photogrammetry for reconstructing the northern part of Santorini’s caldera wall (Fig. 1) for subsequent geological studies. The wall represents an outstanding vertical outcrop of layered deposits dissected by a well-exposed local dyke swarm (Figs. 2a-b). It is characterized by extreme logistic conditions preventing efficient field and UAV surveys due to its steepness and elevation (max height of 330 m a.s.l.).

2 GEOLOGICAL BACKGROUND

The Santorini Volcanic Complex is located in the Aegean Sea and represents the westernmost part of the active Greek volcanic arc (Le Pichon and Angelier, 1979). It is an active stratovolcano composed of five islands (Fig. 1) that were initially united, before multiple (at least four) caldera collapse events formed the currently flooded caldera morphology (Druitt, 2014) (e.g. Fig. 2a).

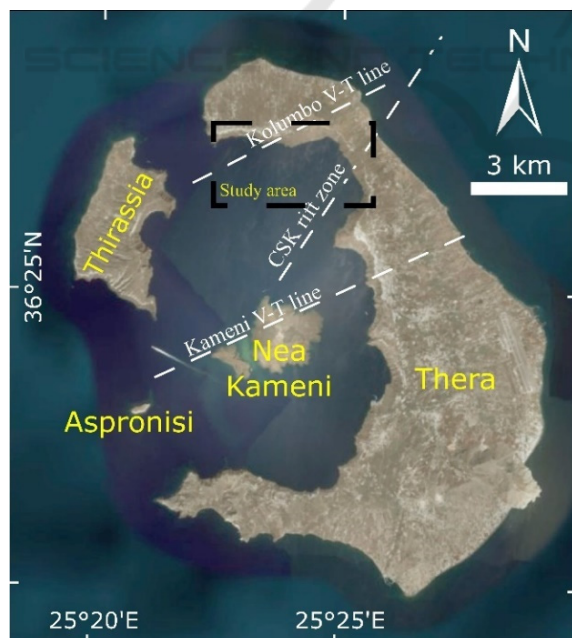


Figure 1: Satellite view of Santorini volcanic complex; the major islands and volcanotectonic lineaments are shown (CSK - Christiana-Santorini-Kolumbo).

Previous studies (Druitt et al., 1999; Rizzo et al., 2015; Hooft et al., 2017) suggest the existence of three volcanotectonic lineaments (Kameni line, Kolumbo line and the Christiana-Santorini-Kolumbo rift zone) which dissect the island and control magma ascent in the shallow crust. Although volcanic activity has been ceased since 1950, the 2011-2012 unrest episode showed magma accumulation beneath the Nea Kameni island (Parks et al., 2012) while the intense seismic activity along the Kameni V-T line exhibited a possible resurgence which, however, did not feed an eruption (Browning et al., 2015). The stratigraphy of the northern part of the caldera wall indicates a large sequence of effusive/explosive subaerial volcanic activity with a variety of volcanic products, and in particular lavas, scoria, tuffs and hyaloclastites (Druitt et al., 1999) (Fig. 2b).

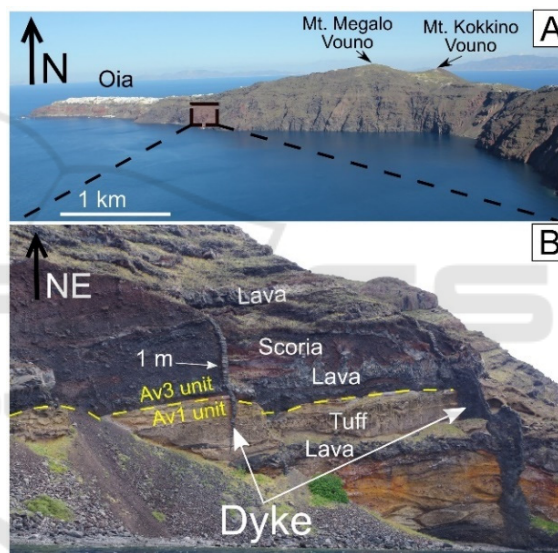


Figure 2: (A) View of the northern caldera wall; the Oia village, as well as Mt Megalo and Kokkino Vouno, are highlighted. (B) Dykes dissect the heterogeneous host rock. Av1 unit: andesitic lavas, tuffs, breccia, and hyaloclastites. Av3 unit: thinly bedded andesitic and basaltic lavas with subordinate dacites, tuffs and scoria.

The basement lithologies belong to the Peristeria stratovolcano (active 530-430 ka) and are capped by the products of two later explosive cycles (360-3.6 ka). The Minoan Plinian eruption ignimbrite lies atop. The dyke-fed eruptions are attested by a local radial dyke swarm of ≥ 90 segments that are visible on the caldera wall and reflect the magmatic and volcanotectonic evolution of the volcano’s plumbing system (Drymoni, 2020). The dykes follow variable paths, and many cross-cutting relationships are observed. Many arrested, deflected, and feeder-dykes

occur and dissect dissimilar mechanically layers (Drymoni et al., 2020).

3 3D MODELLING

In this section, we describe the workflow through which we applied the SfM techniques (e.g. Westoby et al., 2012; Pepe and Prezioso, 2016; Bliakharskii and Florinsky, 2018), which is subdivided into two main steps: *i*) Boat survey and picture collection; and *ii*) SfM photogrammetry processing. The final results are provided in the form of VOs, DSMs, and an Orthomosaic.

3.1 Boat Survey and Picture Collection

Instead of using a commercial UAV, we collected 887 pictures using a static camera, the Sony HX400V bridge model, equipped with the Sensor CMOS Exmor R® 1/2.3" (7.82 mm), 20.4 megapixel, capable of providing GPS tagged photos (Geographic coordinates/Datum WGS84), camera lens ZEISS Vario-Sonnar® T* and $\phi 55$. The operator took the pictures by keeping the camera parallel to the "ground" and opposite to the caldera wall. Adjusted camera settings were used, such as a Sport capture mode and a constant focal length set to 4.34 mm. The boat navigated along a 5.5 km track parallel to the caldera wall from the W to the E-ESE, keeping a constant speed of 4m/s (Fig. 3). The duration of the boat survey was 25 mins, and the horizontal distance range from the coastline was between 35.8 and 296.5 m (Fig. 3), with an average of 144.1 m (SD=70 m). The Z value of each picture was corrected to a value of 4.5 m a.s.l, resulting from GPS Real-time kinematic (RTK) data recording.

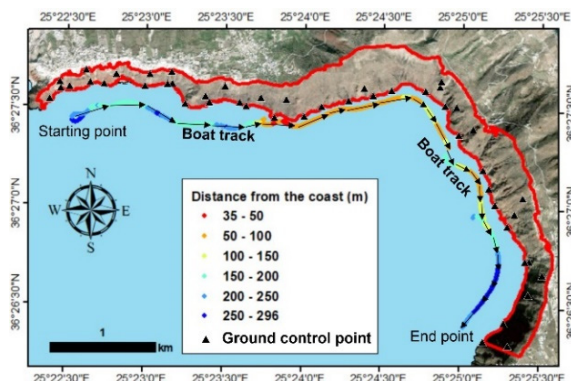


Figure 3: Location of the collected pictures, with their distance from the coast classified in 50m-length intervals. The red curve highlights the area of interest, the boat track is indicated by black arrows.

3.2 Photogrammetry Processing

The workflow continued with photogrammetry processing. All pictures were managed through the Agisoft Metashape (<http://www.agisoft.com/>) photogrammetric software, which processes digital images and generates 3D spatial data, providing a high quality of point clouds (Burns et al., 2017). At a general level, we followed the workflow used in Bonali et al. (2020): *i*) picture alignment and sparse cloud generation; *ii*) dense cloud building; *iii*) VO, DSM and Orthomosaic generation. Firstly, the pictures were uploaded and edited individually to mask all the areas external to the caldera wall (sky and sea) (Fig. 4), to achieve a better processing.

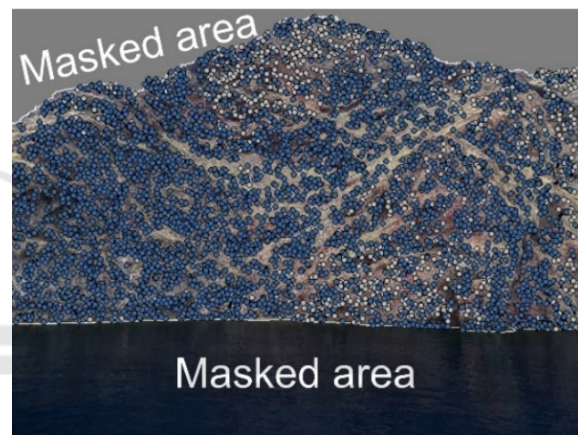


Figure 4: Masked picture; some commonly recognised points by the software are also shown.

The next step consisted in getting an initial low-quality photo alignment by considering only the measured camera locations. Eventually, all the photos with quality value < 0.8 (or out of focus - visual revision) were excluded from any further processing. To allow for the co-registration of datasets and the calibration of models resulting from SfM photogrammetry processing, we added 50 Ground Control Points (GCPs), (e.g. Westoby et al., 2012; James et al., 2017), all provided with 1 m of accuracy. We considered the latitude and longitude values from georeferenced aerial photos and the elevation values from previous high-resolution models designed by the National and Kapodistrian University of Athens. After this step, we re-processed the alignment to obtain better quality. Regarding the alignment, we tested a total of 16 different approaches, considering the following features: *i*) High and Medium accuracy; *ii*) Generic and/or Reference preselection, as well as none of them; *iii*) Key/Tie Point limit set to 40,000/4,000 and 100,000/10,000 respectively. For each, the dense cloud

was generated with Medium accuracy and Mild depth filtering. After these steps, we selected the most efficient approach, considering the overall total length of the processing time and the number of points of the produced dense cloud. The most efficient approach to generate the dense cloud was finally found to be the Alignment with Medium accuracy and both Generic and Reference selection activated (Fig. 5); the pictures overlap ratio is always greater than 90%.

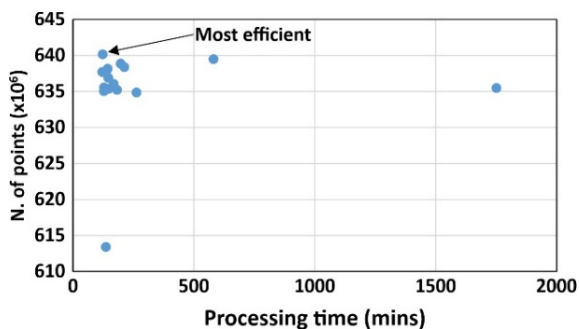


Figure 5: Graph showing the processing time vs the number of dense cloud points, for the 16 different processing approaches.

The duration of the aforementioned step was 121 mins, and the produced dense cloud had 63,770,936 points. Processing was performed using the Agisoft Cloud beta service, from a virtual machine equipped with the following features: a CPU-32 vCPU (2.7 GHz Intel Xeon E5 2686 v4), a GPU 2 × NVIDIA Tesla M60, a RAM 240 GB. We also applied the “Filter by Confidence” tool to remove noisy points from the dense cloud. Primarily, we removed all the points from the overall dense cloud in the range between 0–1 and took out the ones which did not relate to the final area and the model we wished to obtain. On the resulting dense cloud, composed of 56,961,232 Points (Fig. 6), we first generated the DSM model, where the Projection was set up to WGS84 / UTM zone 35N, with interpolation both set to disabled and enabled. Finally, we assigned the Orthomosaic feature with the following “Average setting” as Blending mode, and we kept the “Enable hole filling” disabled, instead of the “Mosaic” as it is usually done with UAV-captured pictures.

3.3 VOs Building

Regarding the VOs and the 3-D produced models, the overall model was built as a tiled model with a Tile size of 4096x4096 pixels and a medium face count. This was suggested by Tibaldi et al. (2020), who proposed to use the Tiled Model as a Virtual Reality scenario. Some parts were also selected and shared

online for further dissemination activities. In detail, to create VOs of adequate quality for online sharing, we suggest the following steps. The first step is to build the mesh from the dense cloud, with an Arbitrary 3D surface type, and 2,100,000 number of faces. Afterwards, it is necessary to create the texture, in two separated files, with a tile size of 4096x4096 pixels; then, the 3-D model can be exported in Collada file format. The output is composed of three files, one for the mesh (DAE file extension) and two for the texture (jpg file extension) (Fig. 7a). The online shared model is shown in Figure 7b.

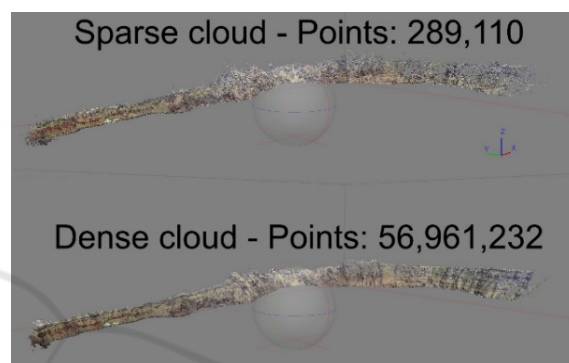


Figure 6: Best sparse and dense cloud obtained with the workflow mentioned above, including a “Filter by confidence” tool.

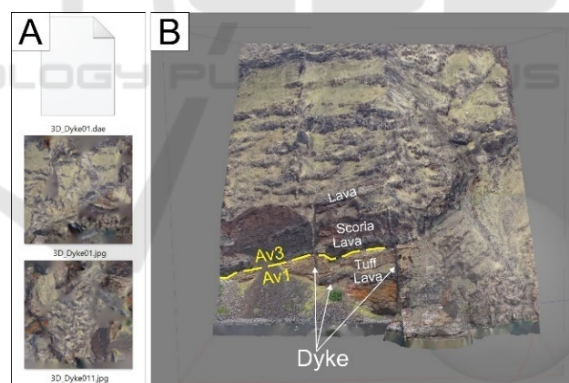


Figure 7: (A) DAE file for the mesh and the two JPG files of the texture feature needed for the 3D model (B). Av3 and Av1 units as well as the dykes and the observed crustal segment are explained in detail in the caption of Figure 2.

4 RESULTS

4.1 DSMs and Orthomosaic

We collected a total number of 877 pictures to be used during the photogrammetry processing to build up the DSM and the Orthomosaic. The size of the research

area was measured with the ArcGIS Pro tools and was found to cover 1.84 km² (Fig. 3). The DSM, processed without using interpolation settings, covered an area of 1.25 km², that is 30 % smaller than the target area, resulting in a resolution of 22.3 cm/pix and an elevation range from -2.68 to 311.77 m a.s.l. (Fig. 8a). The DSM processed using interpolation settings had the same pixel size, covered the entire target area, and showed an elevation range from -3.0 to 314.5 m a.s.l. (Fig. 8b). The processing time of the two DSMs was 3 mins and 22 mins, respectively.

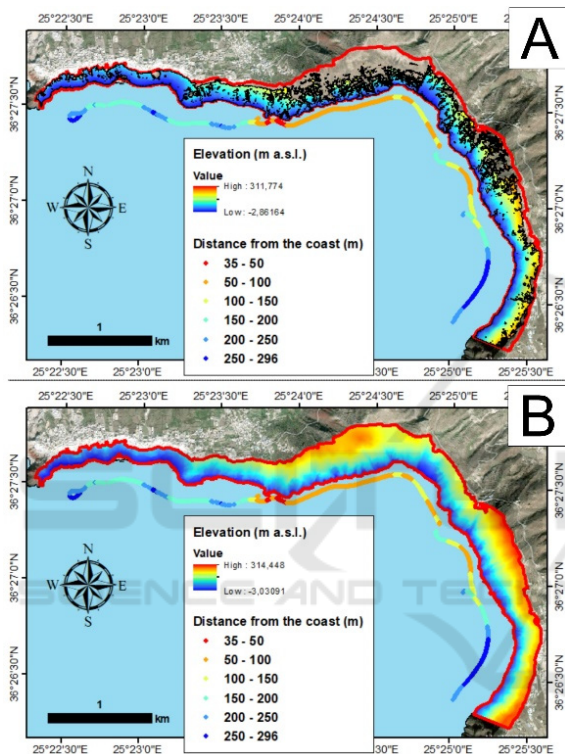


Figure 8: DSMs derived by photogrammetry processing limited to the target area (red area), built without (A) and with interpolation settings selected (B).

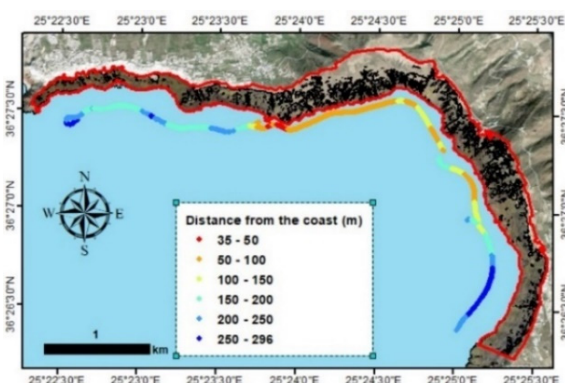


Figure 9: Orthomosaic derived by photogrammetry processing restricted to the target area (red area).

The 5-m-resolution DEM provided by the National Cadastre & Mapping Agency S.A. is in the range of 2.20 - 329.23 m a.s.l.. Regarding the Orthomosaic, it has the same areal coverage as the first DSM, no interpolation settings were selected, and has a resolution of 5.8 cm/pix (Fig. 9). Its processing time was 493 mins. To define the research area, we first calculated a ridgeline. We used the 5-m-resolution digital elevation model (DEM) derived from the area's orthophoto map (2012) of the National Cadastre & Mapping Agency S.A. in ArcGIS Pro, to create the flow direction initially and then the flow accumulation raster files by applying the DINF method, that uses the steepest slope of a triangular facet. Then, we reclassified the flow accumulation file into two classes separating the zero value areas from the rest, isolating the ridgeline area. We then converted the reclassified raster file to a vector one, creating the required ridgeline. Finally, using the orthophoto map of the area, we modified the ridgeline as well as the coastline excluding the residential areas.

4.2 3-D Tiled Model and VOs

We produced the overall 3D Tiled model in 270 mins, and the texture resolution was similar to the Orthomosaic value, i.e. 5.8 cm/pix (Fig. 10a). Similarly to the DSMs and the Orthomosaic, in terms of planar areal extent, the covered area is the same. However, differently from the Orthomosaic and the DSMs, in the 3D Tiled Model all the vertical parts of the caldera, which could be mapped on 2D models, are very well represented, as shown in detail in Figs. 10b-c and from the VO displayed in Figure 7b.

4.3 Relationship between Camera Location and the Derived Models

Even though this is a first approach, our models generally showed a positive correlation between the operator-coast distance and the most representative elevation values in the derived DSM (no interpolation - Fig. 8a). However, in the western and southeastern part of the caldera, the images were collected from a longer distance, so the elevation values were portrayed in a better way (both in terms of their areal coverage and maximum elevation) in the produced DSM and complied with specific conditions. These conditions allowed us to estimate the most representative operator-coast distance vs best-performed elevation above sea level solutions which were: *i*) for ≤ 100 m operator-coast distance, elevation values were between 0-60m, *ii*) for 100-200m

operator-coast distance, a maximum elevation of 150-200m could be reached, *iii*) for >200m operator-coast distance the elevation values could be suitable for the whole model (313m maximum vertical altitude). The above specifications are crucial to plan further similar field campaigns in such extreme conditions. Therefore, we designed a protocol to preliminarily describe the relationship between these realistic field parameters (operator-caldera distance and elevation), which can still be improved. First, we calculated the point density of the DSM data. Then, we selected an upper elevation limit value wherever the derived density was high (0.02 km²; Fig. 11). This allowed the model to trace the most representative solutions. We used such limit as a parameter towards the minimum net (3D) distance calculation between this upper limit and the camera, with information sampling each 1 m along the line (Fig. 11). We show this relationship in Figure 12, where the Maximum Elevation reachable (y-axes) is a function of the 3D distance multiplied by 0.4393 minus 1.7881.

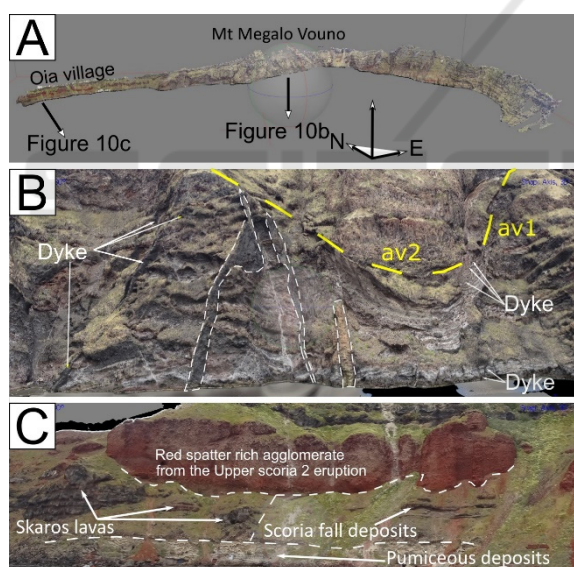


Figure 10: (A) The resulting 3D Tiled Model. (B) 3D model view of the area below Mt Megalo Vouno. The dykes were emplaced into a heterogeneous and anisotropic host rock, which belongs to the oldest local volcanic activity (Peristeria stratovolcano, 530-430 ka), and dissected the bottom units: *i*) av1 - a mixture of andesitic lavas, tuffs, breccias, and hyaloclastites; *ii*) av2 - silicic andesitic lavas. (C) 3D model view of the caldera wall at Oia village.

5 DISCUSSION

Here, we critically discuss the application of our proposed methodological approach to the VOs,

DSMs and Orthomosaic design in extreme conditions where the use of UAVs is difficult for image collection. We have designed a safe, user-friendly, economic and well-developed approach to build up 3D models aimed at overcoming field-related challenges but, most importantly, tackling the technical limitations and methodological impact on the interpretation of the findings, which could not be addressed by other techniques. Our well-tested methodology proposes that the resolution produced by the SfM-derived DSMs and Orthomosaic is well portrayed and successfully serves the scopes of geological interpretation and quantitative and qualitative data collection for geoscientists.

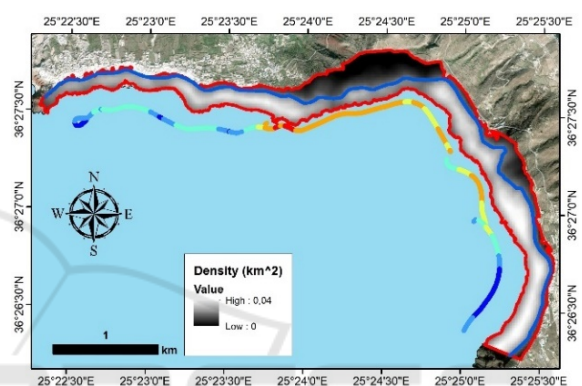


Figure 11: Map showing the point density values calculated by the DSM, with no interpolation settings. The blue line represents the upper elevation selected limit.

We also critically consider that the difference between the 5-m DSM and the SfM derived model (interpolation settings were inactive) can produce good correlations for the used scale (km range) of our study. Our results show a major difference between the elevation values produced by the two models (Fig. 13), ranging from -63.19 to 52.32 m, mean value = -0.09. However, their statistical analysis implies a much lower standard deviation (SD) value than its broad range, suggesting instead that the majority of data are within an SD of 9.95. To obtain results with a better statistical performance, we propose an updated scenario which offers: 1) high precision GCPs, 2) a UAV-based mission in conjunction with this methodology to complement the collected picture set considering different cliff and elevation angles. This can increase the quality of the produced DSM and provide more accurate structural data. We have also tested an identical scenario and have designed a DSM by activating the interpolation settings. The statistical analysis shows a broader range of values as well as a greater standard deviation (SD) than in the previous case; the range is between -62.44 and 98.56,

the mean is 3.02 and the SD = 13.24 (Fig. 14). Furthermore, we noticed that both the over and underestimated elevation values belonged to pictures collected very close to the coast.

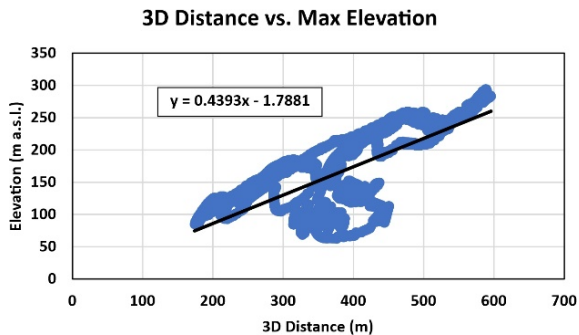


Figure 12: Graph showing the relation between the 3D distance from the camera and the maximum reachable and reliable elevation in the DSM.

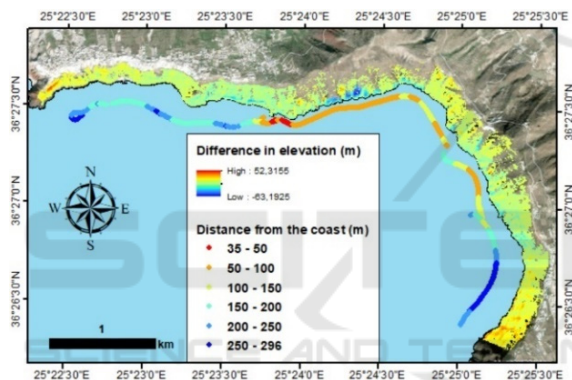


Figure 13: Raster showing the difference in elevation between the 5-m DSM and the SfM-derived DSM obtained with no interpolation settings.

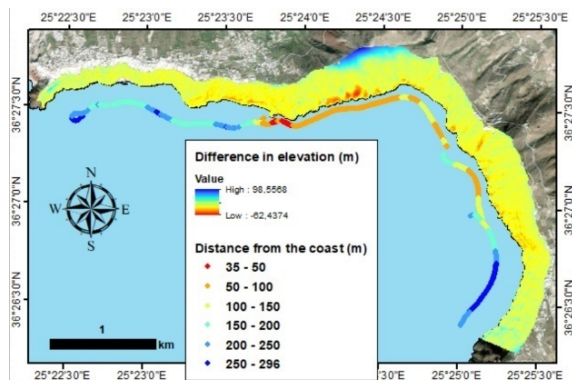


Figure 14: Raster showing the elevation difference between the 5-m DSM and the SfM-derived DSM obtained with active interpolation setting.

Finally, although the Orthomosaic suffered from significant distortion effects due to the high slope

morphology of the target area, the 3D Tiled model, as well as the selected VOs, show some excellent vertical outcrops. The above considerations prove that the proposed technique can be used for research surveys and data collection protocols; such activities were once instead impossible to carry out with sufficient precision, owing to accessibility limitations (e.g. Fig. 7). For example, our methodology gave satisfying results in relation to the quantitative measurements of dyke thickness, as shown in Figs. 2b and 7. The data of this campaign and especially the ones related to dyke thickness measured by Drymoni et al. (2020) in Figs 2b and 7 have been compared with our derived 3D model, showing excellent overlap. Similarly, we refer to the comparisons between another dyke studied by Tibaldi et al. (2020) and our 3D model. The results show, once again, a centimetric difference between the two thickness measurements. Such observations suggest the practicality, but most importantly the level of confidence of the SfM-derived 3D models proposed here, for data collection and 3D geological reconstructions. Finally, the overall 3D models, as well as their selected parts, can be excellent teaching resources and could serve significantly as part of interactive outreach activities. In this regard, we aim to enhance the accessibility of the northern caldera wall, publishing three sites as “Virtual Outcrops” (e.g. Pasquaré Mariotto et al., 2020) available on the webpages: <https://geovires.unimib.it/geovolc/> and <https://geovires.unimib.it/shallow-magma-bodies/>, where a scientific description is also provided for each model. Finally, as suggested by Tibaldi et al. (2020), the SfM-derived 3D Tiled model can be imported in a game engine, building fully navigable immersive VR systems (<https://www.geavr.eu/>).

6 CONCLUSIONS

In the present work, we achieved the following outcomes: *i*) a major, high-resolution 3D tiled model with a texture resolution of 5.8 cm/pix, *ii*) two DSMs and an Orthomosaic with a pixel resolution of 22.3 and 5.8 cm/pix respectively, *iii*) a series of VOs for dissemination activities. More importantly, we applied the aforementioned SfM photogrammetry approach in extreme conditions, providing a preliminary equation that can be used to plan further surveys along the almost vertical and inaccessible cliff, using a static camera to run the pictures collection task.

ACKNOWLEDGEMENTS

Funding is from : *i*) the ILP-Task Force II (Leader A. Tibaldi); *ii*) the MIUR project ACPR15T4_00098–Argo3D (<http://argo3d.unimib.it/>); *iii*) the Virtual Diver project (<https://www.virtualdiver.gr/>); *iv*) NEANIAS project (<https://www.neanias.eu/>). Special thanks to Captain Giorgos Renieris of the Santorini Boatmen Union. Agisoft Metashape is acknowledged for photogrammetric data processing. Finally, this paper is an outcome of GeoVires lab (<https://geovires.unimib.it>).

REFERENCES

- Bliakharskii, D. P., & Florinsky, I. V. (2018, March). Unmanned aerial survey for modelling glacier topography in Antarctica: first results. In GISTAM (pp. 319-326).
- Bonali, F. L., Tibaldi, A., Corti, N., Fallati, L., & Russo, E. (2020). Reconstruction of Late Pleistocene-Holocene Deformation through Massive Data Collection at Krafla Rift (NE Iceland) Owing to Drone-Based Structure-from-Motion Photogrammetry. *Applied Sciences*, 10(19), 6759.
- Browning, J., Drymoni, K., Gudmundsson, A., (2015). Forecasting magma-chamber rupture at Santorini volcano, Greece. *Scientific reports*, 5, 15785.
- Burns, J. H. R., & Delparte, D. (2017). Comparison of commercial structure-from-motion photogrammetry software used for underwater three-dimensional modeling of coral reef environments. *The International Archives of Photogrammetry, Remote Sensing and Spatial Information Sciences*, 42, 127.
- Druitt, T.H., Edwards, L., Mellors, R.M., Pyle, D.M., Sparks, R.S.J., Lanphere, M., Davis, M., Barriero, B., (1999). Santorini Volcano. *Geological Society Memoir No. 19*, 165.
- Druitt, T. H., (2014). New insights into the initiation and venting of the Bronze-Age eruption of Santorini (Greece), from component analysis, *Bull. Volcanol.*, 76, 794
- Drymoni, K., Browning, J., Gudmundsson, A., (2020). Dyke-arrest scenarios in extensional regimes: Insights from field observations and numerical models, Santorini, Greece, *Journal of Volcanology and Geothermal Research*, 396, 106854
- Drymoni, K., (2020). Dyke propagation paths: The movement of magma from the source to the surface, PhD thesis, Royal Holloway University of London, UK
- Fallati, L., Saponari, L., Savini, A., Marchese, F., Corselli, C., & Galli, P. (2020). Multi-Temporal UAV Data and object-based image analysis (OBIA) for estimation of substrate changes in a post-bleaching scenario on a maldivian reef. *Remote Sensing*, 12(13), 2093.
- Friedrich, W., Kromer, B., Friedrich, M., Heinemeier, J., Pfeiffer, T., Talamo, S., (2006). Santorini eruption radiocarbon dated to 1627–1600 Bc., *Science*, 312, 548
- Gudmundsson, A., 2020. *Volcanotectonics*. Cambridge University Press, Cambridge.
- Hooft, E.E.E., P. Nomikou, D.R. Toomey, D. Lampridou, C. Getz, M. Christopoulou, D. O’Hara, G.M. Arnoux, M. Bodmer, M. Gray, B.A. Heath, and B.P. Vander Beek, (2017). Backarc tectonism, volcanism, and mass wasting shape seafloor morphology in the Santorini-Christiana-Amorgos region of the Hellenic Volcanic Arc, *Tectonophysics*, 712-713, 396-414.
- James, M. R., Robson, S., & Smith, M. W. (2017). 3 - D uncertainty - based topographic change detection with structure - from - motion photogrammetry: precision maps for ground control and directly georeferenced surveys. *Earth Surface Processes and Landforms*, 42(12), 1769-1788.
- Le Pichon, X., Angelier, J., (1979). The Hellenic arc and trench system: A key to the neotectonic evolution of the eastern Mediterranean area. *Tectonophysics*, 60, 1-42.
- Pasquaré Mariotto, F., Bonali, F. L., & Venturini, C. (2020). Iceland, an open-air museum for geoheritage and Earth science communication purposes. *Resources*, 9(2), 14.
- Parks, M.M., Biggs, J., England, P., Mather, T.A., Nomikou, P., Palamartchouk, K., Papanikolaou, X., Paradissis, D., Parsons, B., Pyle D.M., (2012). Evolution of Santorini Volcano dominated by episodic and rapid fluxes of melt from depth, *Nat. Geosci.*, 5, 749-754.
- Pepe, M., & Prezioso, G. (2016, April). Two Approaches for Dense DSM Generation from Aerial Digital Oblique Camera System. In GISTAM (pp. 63-70).
- Rizzo, A.L., Barberi, F., Carapezza, M.L., Di Piazza, A., Francalanci, L., Sortino, F., D’Alessandro, W., (2015). New mafic magma refilling a quiescent volcano: Evidence from He–Ne–Ar isotopes during the 2011–2012 unrest at Santorini, Greece. *Geochemistry, Geophysics, Geosystems*, 16, 798- 814.
- Scott, C., Bunds, M., Shirzaei, M., & Toke, N. (2020). Creep along the Central San Andreas Fault from Surface Fractures, Topographic Differencing, and InSAR. *Journal of Geophysical Research: Solid Earth*, 125(10), e2020JB019762.
- Tibaldi, A., & Bonali, F. L. (2017). Intra-arc and back-arc volcano-tectonics: Magma pathways at Holocene Alaska-Aleutian volcanoes. *Earth-Science Reviews*, 167, 1-26.
- Tibaldi, A., Bonali, F. L., Vitello, F., Delage, E., Nomikou, P., Antoniou, V., & Whitworth, M. (2020). Real world-based immersive Virtual Reality for research, teaching and communication in volcanology. *Bulletin of Volcanology*, 82(5), 1-12.
- Xu, X., Aiken, C.L., Nielsen, K.C., (1999). Real time and the virtual outcrop improve geological field mapping. *Eos, Transactions American Geophysical Union*, 80(29), 317-324.
- Westoby, M. J., Brasington, J., Glasser, N. F., Hambrey, M. J., & Reynolds, J. M. (2012). ‘Structure-from-Motion’ photogrammetry: A low-cost, effective tool for geoscience applications. *Geomorphology*, 179, 300-314.